

Novel efficient techniques for computer simulation of magnetic recording

D. M. News
W. E. Donath
G. J. Martyna
M. E. Schabes
B. H. Lengsfeld III

*Perpendicular recording—a new paradigm for high-density magnetic recording currently under intensive development—presents complex engineering challenges which require that design be assisted by computer simulation. However, simulating perpendicular recording is itself a challenge for several reasons; it requires a large simulation box that includes both write head and hard disk and must be treated at high spatial resolution, and the simulations must run for long periods of time and for numerous data inputs. To accomplish this complex modeling, we have developed novel techniques which involve a mixed real-space/Fourier-space representation and which compute time scales **linearly** with system size, enabling large simulations to be performed efficiently. We show tests of our methodology and provide an example of a simulation that involves writing three bits (a **tribit**) to disk.*

Introduction

In magnetic recording—the central process in storage technology—the write head produces a write magnetic field that imprints its polarization upon the thin-film magnetic recording medium which forms the top layer of the disk. The design of the write head and disk recording medium is assisted by micromagnetic numerical simulation. The rapid increase in areal bit density (currently by a factor of $2\times$ per year) is placing greater demands on all aspects of engineering design [1–3]. The difficulties being encountered may lead to a recording-technology paradigm shift from conventional *longitudinal* recording to *perpendicular* recording [4–8]. Simulating perpendicular recording is more demanding than simulating longitudinal recording and constitutes a major challenge in itself. Meeting this challenge is the subject of extensive current research [9–21].

The paradigm shift in recording technology is motivated by micromagnetic scaling, wherein higher *bit density* is linked to higher *write fields*. In longitudinal recording—the technology embodied in all existing products [1–8, 22, 23]—

the write field lies in the disk plane, and there is a large air gap between the write pole pieces. This geometry keeps the write field relatively weak, which limits the achievable bit density. In perpendicular recording [4–8], a “keeper” layer of highly permeable magnetic material, the *soft underlayer* (SUL), is located between the recording medium and the disk body (**Figure 1**). The effective air gap between the high-permeability SUL and write-head elements of the magnetic circuit can be defined as the physical air gap plus the thickness of the high-coercive-field recording medium. This gap, which the magnetic field must cross, is reduced to a few tens of nanometers, enabling a substantial increase in the write field. The orientation of the written bit now follows the vertical polarization of the magnetic field in the medium (Figure 1), and hence lies perpendicular to the disk; thus, a recording medium with uniaxial anisotropy perpendicular to the disk plane is used.

In perpendicular recording, the write field is strongly dependent on such disk features as SUL properties and recording medium thickness, and it is expected that

©Copyright 2004 by International Business Machines Corporation. Copying in printed form for private use is permitted without payment of royalty provided that (1) each reproduction is done without alteration and (2) the *Journal* reference and IBM copyright notice are included on the first page. The title and abstract, but no other portions, of this paper may be copied or distributed royalty free without further permission by computer-based and other information-service systems. Permission to *republish* any other portion of this paper must be obtained from the Editor.

0018-8646/04/\$5.00 © 2004 IBM

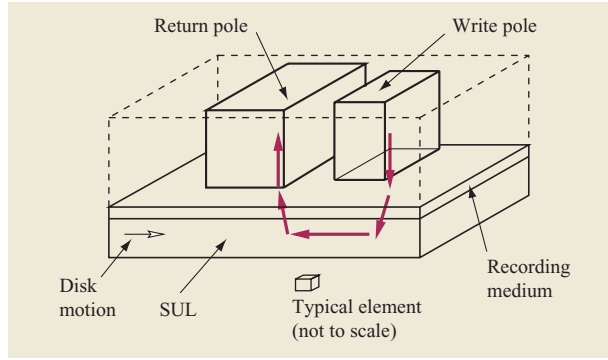


Figure 1

Simulation cell for perpendicular recording showing write head with write and return poles, recording medium (data layer), and soft underlayer (SUL). Red arrows indicate direction of magnetic field, assuming downward direction at write pole.

numerical simulations will be essential to permit the rapid tuning required in engineering design [1–8]. Simulation of the write head and disk combination necessitates including part of the head and a portion of both the recording medium [24, 25] and SUL in the simulation cell (Figure 1). The combined system is relatively large, on the scale of the required resolution, leading to a large number of elements; typically, a simulation cell of dimensions $2560 \times 1280 \times 620$ nm may be required, with a resolution of 2 nm in the recording medium and 10 nm elsewhere, leading to of the order of $N = 3 \times 10^6$ elements. The additional requirements that the simulation be run for about 10^5 time steps with an ensemble of at least 20 independent systems, and for numerous engineering datasets, turn this problem into a major challenge for simulation techniques.

To complete realistic simulations in a usefully short computation time, it is essential that a time step be completed in a linear time of order N or $N \log_2 N$, which we term *scalability*. A range of fundamentally different approaches is currently under investigation to achieve scalability in micromagnetics simulations. These approaches include finite element [9–13], multipole expansion [14–18], and the present technique [20, 21], with historical roots in earlier, not fully scalable, techniques [26–30].

Other applications of micromagnetics, such as to spintronics [31], magnetostrictive actuators [32], and novel approaches to computation [33], may also benefit from the development of scalable computational techniques.

In addition to scalability, the code must also be parallelizable, although large-scale parallelism is not required owing to the existence of the data parallel element of an ensemble of a large number of independent

systems. In this paper we describe the scalable approach to magnetic recording that was developed in collaboration among personnel at the IBM Yorktown and Almaden research facilities. We also include the results of tests and an example of a write simulation.

Micromagnetic modeling

The discretization used in our methodology subdivides the orthorhombic simulation cell into orthorhombic elements which, in the present paper, are taken to be cubic elements of side d (the general methodology [20, 21] allows orthorhombic elements and multigridding). The number of elements in each side of the cell is defined as N_x , N_y , and N_z ; the total number of elements is $N = N_x N_y N_z$. A given element is denoted by the three-dimensional (3D) index $\mathbf{i} = (i_x, i_y, i_z)$, where $0 < i_\alpha < N_\alpha$, and $\alpha = x, y, \text{ or } z$. (Note: Bold typeface indicates terms that are vectorized.) The magnetization (magnetic moment per unit volume) within each element \mathbf{i} is assumed to be a constant, \mathbf{m}_i .

In micromagnetism, the time evolution of the magnetization of each element is controlled by the Landau–Lifschitz–Gilbert (LLG) equation,

$$\frac{d\mathbf{m}_i(t)}{dt} = -|g| \mathbf{m}_i(t) \times \mathbf{H}_i(t) + \frac{\alpha_i}{m_{si}} \mathbf{m}_i(t) \times \frac{d\mathbf{m}_i(t)}{dt}, \quad (1)$$

where g is the gyromagnetic ratio, α_i is the damping constant [34], m_{si} is the saturation magnetization in the material, and \mathbf{H}_i is the effective magnetic field. \mathbf{H}_i consists of the contributions

$$\mathbf{H}_i = \frac{2A}{d^2 m_{si}} \sum_{j \in \text{nn}(i)} \hat{\mathbf{m}}_j + \frac{2K_{ui}}{m_{si}} \tilde{\gamma}(\tilde{\gamma} \cdot \hat{\mathbf{m}}_i) + \mathbf{H}_i^{DM} + \mathbf{H}_i^{ext} \quad (2)$$

and may also include a Langevin noise term [35]. Here the first term is the exchange interaction, with A the exchange constant ($\hat{\mathbf{m}}_i$ is a unit magnetization vector, and $\text{nn} =$ nearest neighbor). The second term is the uniaxial anisotropy, with K_{ui} the anisotropy constant and the unit vector $\tilde{\gamma}$ defining the anisotropy axis. The third term is the long-range dipole–dipole (*demag*) interaction, and the fourth term is the external head field, which drives the write process.

In implementing the computation (Figure 2), the LLG equation is integrated [36] for one time step, updating the magnetization in all elements. Then \mathbf{H}_i is updated, the inputs to this calculation being the set of updated magnetizations $\{\mathbf{m}_i\}$ and the head field at that time step (the head field is a function of the bit sequence to be written and of the relative head–disk velocity).

The computational cost of most of these tasks, the LLG integration, the nearest-neighbor exchange, and the local anisotropy term, are of order N and hence scalable. However, the demag and external head field terms are in

principle order N^2 in computing time and are not scalable. Let us look at the demag field result in more detail.

Demag field

The expression for the demag field is written as a sum in real space,

$$H_{i,\alpha}^{DM} = \sum_{j,\beta} R_{\alpha\beta}(\mathbf{i} - \mathbf{j}) m_{j,\beta}, \quad (3)$$

where

$$R_{\alpha\beta}(\mathbf{i}) = \frac{1}{d^3} \int_{e|0} d^3r \int_{e|i} d^3r' \Phi_{\alpha\beta}(\mathbf{r} - \mathbf{r}'), \quad (4)$$

and, defining $r = \sqrt{x^2 + y^2 + z^2}$,

$$\Phi_{\alpha\beta}(\mathbf{r}) = \frac{\partial}{\partial x_\alpha} \frac{\partial}{\partial x_\beta} \left(\frac{1}{r} \right) = \frac{3x_\alpha x_\beta}{r^5} - \frac{\delta_{\alpha\beta}}{r^3}. \quad (5)$$

Here the “response function” $R_{\alpha\beta}(\mathbf{i})$ is the average magnetic field at element \mathbf{i} caused by the magnetization within element $\mathbf{0}$, located at the origin. The response function $R_{\alpha\beta}(\mathbf{i})$ has been written down analytically for the general case of two equal orthorhombic elements [26–30].

At long range the response function falls off as the inverse cube of distance, a very slow fall-off that necessitates summing over the entire simulation cell, giving unacceptable N^2 scaling for the computation time of the demag field as a real-space sum.

Rapid-convergence approach

A scalable solution to the problem of calculating the demag field \mathbf{H}^{DM} is obtained by splitting up the calculation into a *short-range* part, calculated in real space, and a *long-range* part, calculated in Fourier space. The decomposition is written symbolically as

$$\mathbf{H}^{DM} = \mathbf{h}_R + \mathbf{H}_K, \quad (6)$$

where

$$\mathbf{h}_R = \mathbf{H}^{DM} - \mathbf{H}_K. \quad (7)$$

Here the subscript R implies a sum in real space, and K a sum in Fourier space; \mathbf{h}_R is designed to be a rapidly convergent sum in real space, and \mathbf{H}_K a rapidly convergent sum in Fourier space. The real-space part \mathbf{h}_R is the difference between the true demag field and the Fourier-space part expressed in real space ($\mathbf{H}_R = \mathbf{H}_K$).

In this technique, the long-range (in space) demag interaction is broken up into the sum of two components \mathbf{h}_R and \mathbf{H}_K , both of which are short-range in their respective spaces. However, \mathbf{H}_K primarily takes care of the long-range (in space) piece of the original dipole–dipole interaction, while \mathbf{h}_R primarily takes care of its short-range component. The real-space sum \mathbf{h}_R can be adjusted to fall off as a high inverse power of distance, while the K -space

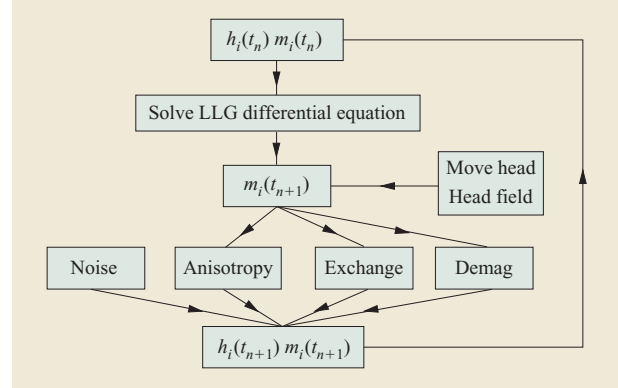


Figure 2

Flow diagram for simulation code.

Table 1 Coefficients for weighting function $\phi(K)$.

τ_p ($d = 1$ unit)	a_p
0.5	252
0.6	−1050
0.7	1800
0.8	−1575
0.9	700
1.0	−126

sum \mathbf{H}_K falls off with a controllable exponential factor. Hence, the combination enables calculation of the demag field with reasonable effort even if high accuracy is demanded.

Real-space part

The real-space part \mathbf{h}_R is derived in the same way as the demag field in Equations (3)–(5) in the foregoing section, except that a newly defined interaction function,

$$\Phi_{\alpha\beta}^R(\mathbf{r}) = \frac{\partial}{\partial x_\alpha} \frac{\partial}{\partial x_\beta} \left\{ \frac{1}{r} - \sum_{p=1}^L \frac{a_p}{\sqrt{x^2 + y^2 + [\tau_p \operatorname{sgn}(z) + z]^2}} \right\}, \quad (8)$$

replaces the dipole–dipole interaction $\Phi_{\alpha\beta}(\mathbf{r})$ in Equation (5). The new interaction function $\Phi_{\alpha\beta}^R(\mathbf{r})$ contains a set of $2L$ arbitrary constants, τ_p and a_p , which are used to control its leading fall-off to the functional form $1/r^{L+3}$. For example, the $L = 6$ parameter set in Table 1 leads to a fall-off in the interaction function as $1/r^9$, which is a vast improvement on $1/r^3$ and is adequately short-range. The response function using the short-range expression (8) is a generalization of the standard one [26–30] and can be expressed analytically [20, 21].

Fourier-space part

A two-dimensional discrete Fourier transform (DFT) is defined in the xy -plane of any given layer i (a layer is normal to the z -axis). We use a notation in which bold capitals, e.g., $\mathbf{I} = (i_x, i_y)$, denote the two-dimensional (2D) index of an element *within* a layer. A function $f_{\mathbf{I}_i}$ is transformed into $f_i(\mathbf{K})$ by the DFT,

$$f_i(\mathbf{K}) = \sum_{\mathbf{I}} e^{i\mathbf{K} \cdot \mathbf{X}_{\mathbf{I}_i}} f_{\mathbf{I}_i}, \quad (9)$$

where the notation $\mathbf{X}_{\mathbf{I}}$ denotes the 2D location $\mathbf{X}_{\mathbf{I}} = \mathbf{I}d$ of the element, and in Fourier space, $\mathbf{K} = 2\pi d^{-1}(m_x/N_x, m_y/N_y)$ (m_α integers) is the 2D wavevector.

In this notation, the Fourier part of the demag field is given by

$$\mathbf{H}_i(\mathbf{K}) = \mathbf{H}_i^+(\mathbf{K}) + \mathbf{H}_i^-(\mathbf{K}) + \mathbf{H}_i^0(\mathbf{K}), \quad (10)$$

where, defining the reciprocal lattice vectors $\mathbf{G} = 2\pi d^{-1}(n_x/n_y)$ (n_α integers), and noting that, from (9), $\mathbf{m}_i(\mathbf{K} + \mathbf{G}) = \mathbf{m}_i(\mathbf{K})$,

$$\begin{aligned} \mathbf{H}_i^\pm(\mathbf{K}) = & -\frac{2\pi}{d^5} \sum_{\mathbf{G}} \phi(|\mathbf{K} + \mathbf{G}|) \mathbf{v}_\pm(\mathbf{K} + \mathbf{G}) h^2(|\mathbf{K} + \mathbf{G}|) \\ & \times f^2(\mathbf{K} + \mathbf{G}) \chi_i^\pm(\mathbf{K} + \mathbf{G}) / |\mathbf{K} + \mathbf{G}| \end{aligned} \quad (11)$$

and

$$\begin{aligned} \mathbf{H}_i^0(\mathbf{K}) = & -\frac{2\pi}{d^5} \sum_{\mathbf{G}} \phi(|\mathbf{K} + \mathbf{G}|) f^2(\mathbf{K} + \mathbf{G}) \\ & \times \left\{ \frac{g(|\mathbf{K} + \mathbf{G}|)}{|\mathbf{K} + \mathbf{G}|} [\mathbf{v}_0(\mathbf{K} + \mathbf{G}) \mathbf{v}_0^T(\mathbf{K} + \mathbf{G})] \mathbf{m}_i(\mathbf{K}) \right. \\ & \left. - 2h(|\mathbf{K} + \mathbf{G}|) m_{iz}(\mathbf{K}) \right\}. \end{aligned} \quad (12)$$

Here, form factors f , h , and g for the cubic element appear,

$$\begin{aligned} f(\mathbf{K}) = & \frac{4 \sin\left(\frac{K_x d}{2}\right) \sin\left(\frac{K_y d}{2}\right)}{K_x K_y}; \\ h(K) = & \frac{1}{K} (1 - e^{-Kd}); \quad g(K) = \frac{2}{K^2} (Kd + e^{-Kd} - 1), \end{aligned} \quad (13)$$

together with vectors defining the divergence (div) operation in this representation,

$$\mathbf{v}_\pm^T = [iK_x, iK_y, \pm K], \quad \mathbf{v}_0^T = [iK_x, iK_y, 0]. \quad (14)$$

The constants τ_p and a_p reappear in the cutoff function

$$\phi(K) = \sum_{p=1}^L a_p e^{-K\tau_p}, \quad (15)$$

in which exponential convergence of the sums (11) and

(12) occurs at the rate $\exp(-K\tau_m)$, τ_m being the minimum of the τ_p .

The quantities $\chi_i^\pm(\mathbf{K})$ are given by the recursion relations

$$\chi_{i\pm 1}^\pm(\mathbf{K} + \mathbf{G}) = \mathbf{v}_\pm^T(\mathbf{K} + \mathbf{G}) \mathbf{m}_i(\mathbf{K}) + e^{-Kd} \chi_i^\pm(\mathbf{K} + \mathbf{G}), \quad (16)$$

with the boundary conditions

$$\chi_0^+(\mathbf{K} + \mathbf{G}) = 0; \quad \chi_{N_z-1}^-(\mathbf{K} + \mathbf{G}) = -|\mathbf{K} + \mathbf{G}| m_{N_z z}(\mathbf{K}). \quad (17)$$

Note that $m_{N_z z}(\mathbf{K})$ is the DFT of the magnetization in the external write head and $N_z - 1$ the top cell layer.

Application

There is a straightforward interpretation of the Fourier results (10–17). In (16), a magnetostatic charge density for a given \mathbf{K} in each layer is created by applying the div operator [i.e., multiplying by the $\mathbf{v}_\pm^T(\mathbf{K})$ vectors] to the magnetization, and the magnetostatic potential from all of the layers is then summed by the recursion relation to give the $\chi_i^\pm(\mathbf{K})$ in each layer. In (11), multiplying by the form factor hf brings in the cubic shape of the elements in which the magnetostatic charge densities are located. The div operator is applied again to obtain the magnetic field from the magnetostatic potential, and finally another factor of hf averages the field over the element.

The demag field is obtained as the sum of the K -space part, the inverse DFT of (10), and the real-space part, (3) and (4) with (8) instead of (5). Numerically, the DFT is performed as a fast Fourier transform (FFT), giving a scaling as $6N \log_2(N_x N_y)$, there being six DFTs. The remaining parts of the K -space part, in particular the recursion relation, scale as N , as does the real-space part, owing to the extremely short range of the real-space interaction. In practice, the fast FFT used [37] is found not to dominate the calculation, which scales almost as N . Note that, by working with magnetostatic potential, the methodology expressed in Equations (10)–(17) gains a factor of 6 relative to methods [26–30] based on magnetic field, in addition to scalability.

Testing the methodology

A complete micromagnetic code, the Almaden–Yorktown Micromagnetic (AYM) simulator, has been developed. The simulator incorporates an LLG equation integrator, all of the local terms in the effective magnetic field \mathbf{H} , and the new scalable approach to calculating the demag field. The real-space response function using (8)—which is a difference formula with short range—is calculated and stored for use at run time in a precomputation step using the exact, analytic formulae derived by us [20, 21].

First, let us check two major assertions: that the novel demag field technique is capable of high accuracy and that computing time scales linearly with system size. Second, we discuss parallelization of the code.

Accuracy and scalability

Figure 3 shows computing cost plotted as a function of demag field accuracy for our rapid-convergence methodology. High accuracies of the order of 10^{-6} are obtainable, with computational cost increasing by a factor of only about 2 for every order of magnitude in accuracy.

In Figure 3, the demag calculation has been implemented for six sets of parameters covering different choices of the ranges in real space (defined by L) and in K space (defined by τ_m). The optimal (lowest curve) choices were a combination of $\tau_m \approx 0.70$, with the real-space cutoff parameter transitioning from $L = 5$ (low requested accuracy) to $L = 7$ (high accuracy), showing that indeed the methodology of breaking up the long-range interaction into real-space and K -space pieces works. The optimal curve in Figure 3 is roughly straight as computer-processing-unit (CPU) time plotted against log of accuracy, showing that computational work increases only linearly, while the specified calculational precision increases exponentially.

In Figure 4 we illustrate the increase in computing time (on a relatively slow machine) with increasing system size. It is seen that the scaling with system size N is almost perfectly linear, the very slight supralinearity being due to the log term arising in the FFT work.

Parallelization

The method used for parallelization in the AYM code is to assign each layer i to a different processor. An advantage of this assignment is that FFT operations, which are intrinsically expensive in terms of communications bandwidth, are local to a processor. With regard to communications, the processors are structured to form a chain connected in the order of the layers i . The most global communication step occurs in the K -space calculation, where the recursion relation for $\chi_i^\pm(\mathbf{K} + \mathbf{G})$ involves passing packets of $2n_G N_x N_y$ words, where n_G is the number of \mathbf{G} vectors in Equations (11) and (12) down the entire chain in both directions.

Figure 5 illustrates results for efficiency of parallelization on various numbers of processors. In Figure 5(a), the parallelization on an IBM scalable parallel (SP*) system is seen to work up to about ten nodes, which is adequate for the present problem since there is a large data-parallel element not included in Figure 5(a), but which in practice will demand multiple nodes. Figure 5(b) represents results for a rather poorly connected system—an Intel** cluster in a 100-Mb/s Ethernet network; parallelization efficiency is poorer than in the SP system case. Analysis shows that bandwidth limitations in the communication system are responsible for the difference.

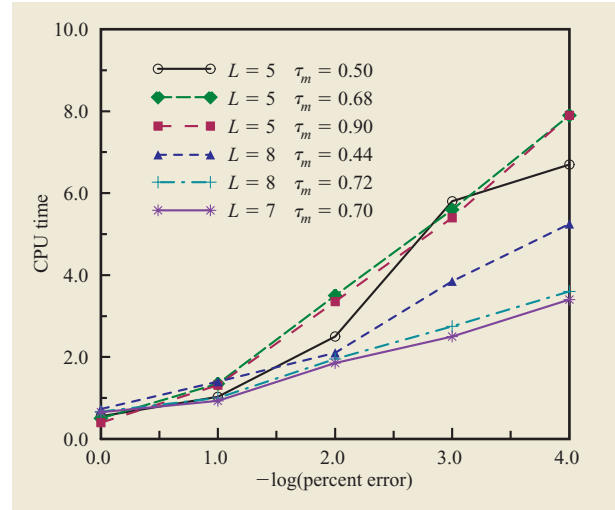


Figure 3

Plot of relative CPU time against $\log_{10}(\text{percent error})$ in rapid-convergence calculation of demag field for various combinations of the rapid-convergence parameters τ_p ($d = 1$ unit) and a_p .

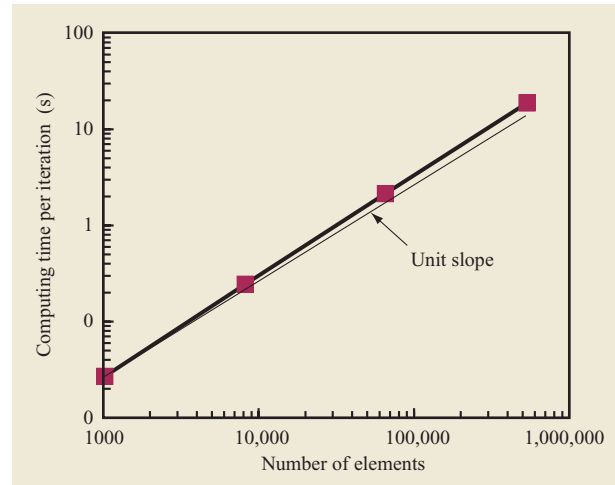


Figure 4

Scaling of computing time with system size, expressed as number of elements.

Summary of tests

It is seen that the rapid-convergence approach indeed achieves high accuracy and that the methodology is scalable with computing time proportional to system size. The parallelizability extends to an order of ten processors, which is adequate because the problems in simulating perpendicular recording involve extensive data

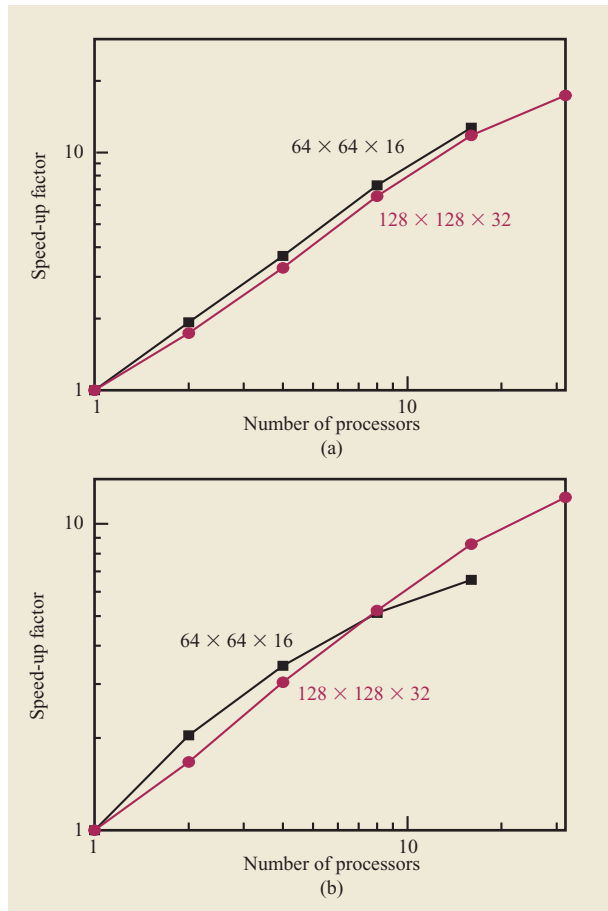


Figure 5

Speed-up factor expressed as the ratio of time on a single node to time on n nodes plotted against n , (a) for an SP system; (b) for an Intel cluster with a 100-Mb/s Ethernet network.

parallelism—a factor of at least 20 for the number of ensemble members. Hence, the AYM code would work well on roughly 200 well-coupled processors.

Simulation of writing a tribit

Specifics of simulation

Realistic simulation of the data-writing process must take into account the specific structure of a typical data layer, the thin-film recording medium shown in Figure 1. Whereas the magnetically homogeneous head material and SUL may be modeled adequately using 10-nm cubic elements, the data layer is a grained material in which the grains have a large degree of magnetic independence of one another. The grain size distribution is log-normal, with an average grain diameter of ~ 10 nm, but the grain shape must be modeled on a grid with a 2-nm resolution

in order to capture the grain morphology. The methodology allows multigridding, but the choice of a 2-nm grid introduces a factor of 25 into FFT computing time within the data layer, raising problems of computing efficiency.

The solution adopted, described in more detail in [21], is again to exploit the mixed K -space/real-space representation in which the demag field is calculated in two pieces, a short- and a long-range piece. In the long-range piece, the magnetization is computed in Fourier space using a relatively coarse grid, such as 10 nm. In the short-range piece, a set of intergrain interactions—calculated to complement the long-range piece so that they sum to the correct result—are precomputed. The intergrain interactions turn out to be short-range, so again the computation is in linear time.

The simulation using the AYM code employs the basic setup illustrated in Figure 1. A write field is applied via (17) as a time-varying charge sheet to the top of the write and return poles where they intersect the upper surface of the simulation cell. A fairly realistic parameter set (see [21]) was employed. Results are presented for a single-member ensemble run on a single 2-GHz Intel processor using a $64 \times 64 \times 14$ -element array with a nonuniform z -spacing, and one grained data layer, for 30,000 time steps, a run that took five hours. The results are presented in Figure 6.

Simulation results

The initial magnetization was taken in the z -direction with polarization up in the data layer, and in the y -direction in the SUL and head layers. This initial condition in the SUL and head accounts for the asymmetric 45° structures generated in the SUL, which were also observed in previous simulations.¹ The results presented in Figure 6 display the z -component of magnetization in the top SUL layer (left column) and the data layer (right column) according to the color codes shown in the legend.

Frame 5 in Figure 6 occurs after the write head has applied a “down” field for a short time and the magnetization in the data layer beneath the write pole has begun to turn over. In the SUL, the “down” magnetic field beneath the write pole is clearly evident, as is also the “up” field beneath the return pole. However, because the return pole has the same z -direction magnetic flux along with a larger area, its magnetic field is insufficient to turn over a significant fraction of the grains in the data layer. This effect is by design. It is important that the return pole not interfere with the write process. In the second time slice, the write field is beginning to turn off [left side of Frame 15], while the negative polarization of the data layer under the write head is complete.

¹ M. E. Schabes and B. H. Lengsfeld III, private communications.

Frames 16 and 23 show phenomena very similar to those just described, except that the write head field is now “up.” The result would be to obliterate the effect of the polarization written when the head field was “down,” but for the fact that the head has now moved to the left. Hence, a negatively polarized region of the data layer survives the magnetization reversal, forming a “down” bit.

Frames 28 and 32 show a repeat of the phenomena in Frames 5 and 15: A “down” head field is reversing the data layer magnetization beneath the write pole. Again due to head motion, an “up” polarized region in the data layer survives the second magnetization reversal, forming the second bit. Finally, in Frame 49, the write field is turned off, leaving behind a tritbit, manifested by the blue/red/blue (down, up, down) pattern in the data layer.

This realistic simulation demonstrates the essential features of perpendicular magnetic recording, the “graininess” of the written bits, the repeatability of the write operation, and the relatively undisturbed nature of the region beneath the return pole. Perpendicular recording is shown to satisfactorily write 64-nm-length bits with appropriate engineering parameters.

The 64×64 -tritbit simulation took five hours of computing time on a 2-GHz personal computer (PC). The time required to implement a full engineering 128×128 simulation with 20 ensembles having statistically independent grain and $\tilde{\gamma}$ distributions in the data layer and independent Langevin noise distributions can be estimated on the basis of the foregoing scaling analyses. We then readily determine that the full simulation would take ten hours on a 40-way cluster built from machines equivalent in performance to the 2-GHz PC. Hence, with reasonable investment, the methodologies we have developed can lead to realistic simulations of the perpendicular recording write process *overnight*. It is clearly possible to test designs using detailed computational studies of perpendicular recording.

Concluding remarks

In this paper, a new suite of techniques is presented for improving the efficiency and accuracy of simulations of the perpendicular magnetic recording technology. The new methods were designed specifically to improve the calculation of the demag field in layered magnetic materials and to make the fast, efficient simulation of perpendicular magnetic recording feasible for sufficiently small computational cost so that many designs and materials can be tested. First, the accuracy, efficiency, and parallel scaling of the new techniques were demonstrated on challenging model problems designed to probe for weaknesses. The AYM code was then employed to perform a full-scale simulation of perpendicular magnetic recording, a nanoscale machine writing a tritbit in a grained data layer, clearly demonstrating the applicability

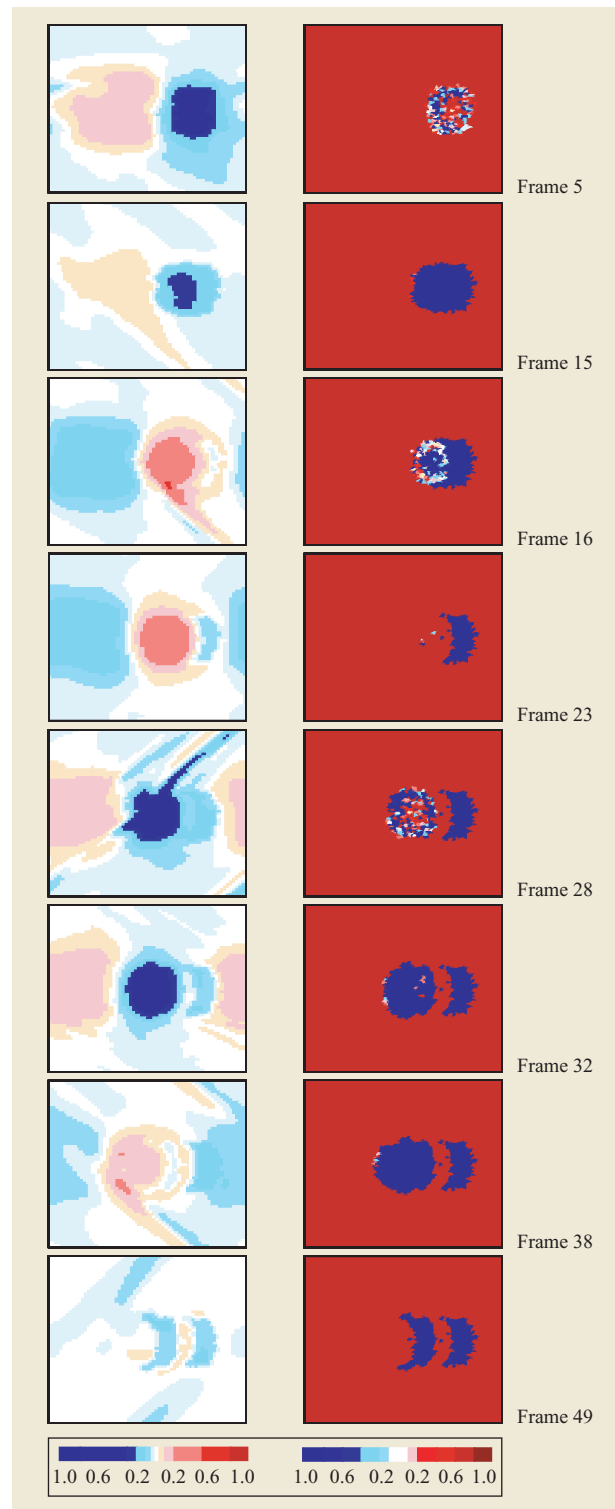


Figure 6

Simulation of recording a tritbit. Left column: z -magnetization in the top SUL layer. Right column: z -magnetization in the data layer. The frames, separated by 500 time steps, are in sequential time order starting from the top.

of the techniques to challenging and important technological problems.

Indeed, with a reasonable-sized PC cluster or IBM SP system, it is now possible to simulate the perpendicular recording process and, for example, to obtain overnight engineering statistics of the written bit profile.

*Trademark or registered trademark of International Business Machines Corporation.

**Trademark or registered trademark of Intel Corporation.

References

1. R. W. Wood, J. Miles, and T. Olson, "Recording Technologies for Terabit Per Square Inch Systems," *IEEE Trans. Magn.* **38**, No. 4, 1711–1718 (July 2002).
2. Kai-Zhong Gao and H. N. Bertram, "Magnetic Recording Configuration for Densities Beyond 1 Tb/in.² and Data Rates Beyond 1 Gb/s," *IEEE Trans. Magn.* **38**, No. 6, 3675–3683 (November 2002).
3. D. Wei, H. N. Bertram, and F. Jeffers, "A Simplified Model of High Density Tape Recording," *IEEE Trans. Magn.* **30**, No. 5, 2739–2749 (September 1994).
4. M. E. Schabes, B. Lengsfeld, and T. Schrefl, "Micromagnetic Modeling of Soft Underlayer," *IEEE Trans. Magn.* **38**, No. 4, 1670–1675 (July 2002).
5. J. Xue and R. H. Victora, "Micromagnetic Calculation for Superlattice Magnetic Recording Media," *J. Appl. Phys.* **87**, No. 9, 6361–6363 (May 2000).
6. R. H. Victora, W. Peng, J. Xue, and J. H. Judy, "Superlattice Magnetic Recording Media: Experiment and Simulation," *J. Magn. & Magn. Mater.* **235**, No. 1/3, 305–311 (October 2001).
7. R. Khan and R. H. Victora, "Micromagnetic Model of Perpendicular Recording Head with Soft Underlayer," *IEEE Trans. Magn.* **37**, No. 4, 1379–1381 (July 2001).
8. E. Champion and H. N. Bertram, "The Effect of MR Head Geometry on Playback Pulse Shape and Spectra," *IEEE Trans. Magn.* **31**, No. 4, 2461–2470 (July 1993).
9. T. Schrefl, M. E. Schabes, and B. Lengsfeld, "Fast Reversal Dynamics in Perpendicular Magnetic Recording Media with Soft Underlayer," *J. Appl. Phys.* **91**, No. 10, 8622–8665 (May 2002).
10. J. Fidler, T. Schrefl, V. D. Tsiantos, W. Scholz, D. Suess, and H. Forster, "Ultrafast Switching of Magnetic Elements Using a Rotating Field," *J. Appl. Phys.* **91**, No. 10, 7974–7976 (May 2002).
11. D. Suess, V. Tsiantos, T. Schrefl, W. Scholz, and J. Fidler, "Nucleation in Polycrystalline Thin Films Using a Preconditioned Finite Element Method," *J. Appl. Phys.* **91**, No. 10, 7977–7979 (May 2002).
12. I. A. Tsukerman, A. Plaks, and H. N. Bertram, "Multigrid Methods for Computation of Magnetostatic Fields in Magnetic Recording Problems," *J. Appl. Phys.* **83**, No. 11, 6344–6346 (1998).
13. R. Dittrich, T. Schrefl, H. Forster, D. Suess, W. Scholz, J. Fidler, and V. Tsiantos, "Finite Element Simulation of Discrete Media with Granular Structure," *IEEE Trans. Magn.* **38**, No. 5, 1967–1969 (September 2002).
14. D. M. Apalkov and P. B. Visscher, "Application of Fast Multipole Method to Micromagnetic Simulation of Periodic Systems," *IEEE Trans. Magn.* **39**, 3478 (2003).
15. G. Brown, M. A. Novotny, and P. A. Rikvold, "Micromagnetic Simulations of Thermally Activated Magnetization Reversal of Nanoscale Magnets," *J. Appl. Phys.* **87**, No. 9, 4792–4794 (2000).
16. L. Greengard, *The Rapid Evaluation of Potential Fields in Particle Systems*, MIT Press, Cambridge, MA, 1988.
17. L. Greengard and V. Rokhlin, "A Fast Algorithm for Particle Simulations," *J. Comp. Phys.* **73**, No. 2, 325–348 (December 1987).
18. J. J. Miles and B. K. Middleton, "A Hierarchical Micromagnetic Model of Longitudinal Thin Film Recording Media," *J. Magn. & Magn. Mater.* **95**, 99–108 (1991).
19. J. J. Miles, B. K. Middleton, and C. J. Rea, "High Frequency Magnetization Reversal in Rotating Fields," *IEEE Trans. Magn.* **37**, No. 4, 1366–1368 (July 2001).
20. D. M. Newns, W. E. Donath, G. J. Martyna, M. E. Schabes, B. E. Lengsfeld, and T. Schrefl, "High Performance Scientific and Engineering Computing with Applications," *Proceedings of PDSECA'02 (workshop of IPDPS)*, 2002; to appear in a special issue of *Parallel Algorithms and Applications* (2004).
21. D. M. Newns, W. E. Donath, G. J. Martyna, M. E. Schabes, and B. E. Lengsfeld, "Efficient Techniques for the Computer Simulation of Magnetic Recording in Complex Layered Materials," *J. Appl. Phys.* (2004).
22. S. X. Wang and A. M. Taratorin, *Magnetic Information Storage Technology*, Academic Press, Inc., New York, 1999.
23. H. N. Bertram, *Theory of Magnetic Recording*, Cambridge University Press, Cambridge, England, 1994.
24. A. D. Liu and H. N. Bertram, "Modeling the Effect of Interactions in Granular Magnetic Films," *J. Appl. Phys.* **89**, No. 5, 2861–2869 (2001).
25. J. R. Hoinville, "Thermal Decay of Longitudinal Recording Media with Irregular Grain Shapes," *IEEE Trans. Magn.* **37**, No. 4, 1350–1353 (July 2001).
26. H. Zhou, H. N. Bertram, and M. E. Schabes, "Micromagnetic Analysis of the Effect of Intergranular Exchange on Thermal Stability in Magnetic Recording. III. Perpendicular Media," *IEEE Trans. Magn.* **38**, No. 2, 1422–1428 (March 2002).
27. S. W. Yuan, "Micromagnetics of Domains and Walls in Soft Ferromagnetic Materials," Ph.D. thesis, University of California at San Diego, 1992, pp. 25–33.
28. M. E. Schabes and H. N. Bertram, "Magnetization Processes in Ferromagnetic Cubes," *J. Appl. Phys.* **64**, No. 3, 1347–1357 (August 1988).
29. M. E. Schabes and A. Aharoni, "Magnetostatic Interaction Fields for a Three-Dimensional Array of Ferromagnetic Cubes," *IEEE Trans. Magn.* **23**, No. 6, 3882–3888 (November 1987).
30. R. H. Victora and M. Khan, "Micromagnetic Model of Perpendicular Head and Double-Layer Media for 100 Gb/in.²," *IEEE Trans. Magn.* **38**, No. 1, 181–184 (January 2002).
31. R. H. Koch, J. G. Deak, D. W. Abraham, P. L. Trouilloud, R. A. Altman, Y. Lu, W. J. Gallagher, R. E. Scheurlein, K. P. Roche, and S. S. P. Parkin, "Magnetization Reversal in Micron-Sized Magnetic Thin Films," *Phys. Rev. Lett.* **81**, No. 20, 4512–4515 (1998).
32. X. Tan, J. S. Baras, and P. S. Krishnaprasad, "Fast Evaluation of Demagnetizing Field in Three Dimensional Micromagnetics Using Multipole Approximation," *Smart Structures and Materials 2000: Mathematics and Control in Smart Structures*, V. V. Varadan, Ed., *Proc. SPIE* **3984**, 195–201 (2000).
33. P. R. Kotiuga and T. Toffoli, "Potential for Computation in Micromagnetics via Topological Conservation Laws," *Physica D* **120**, 139–161 (1998).
34. S. Ingvarsson, L. Ritchie, X. Y. Liu, Gang Xiao, J. C. Slonczewski, P. L. Trouilloud, and R. H. Koch, "Role of Electron Scattering in the Magnetization Relaxation in Thin Ni₈₁Fe₁₉ Films," *Phys. Rev. B* **66**, 214416–214421 (2002).
35. O. Chubykalo, R. Smirnov-Rueda, J. M. Gonzalez, W. A. Wongsam, R. W. Chantrell, and U. Nowak, "Brownian

Dynamics Approach to Interacting Magnetic Moments,” *Phys. Rev. B* **67**, 064422–064432 (2003).

36. X.-P. Wang, C. J. Garcia-Cervera, and E. Weinan, “A Gauss–Seidel Projection Method for Micromagnetics Simulations,” *J. Comp. Phys.* **171**, 357–372 (2001).
37. M. Frigo and S. G. Johnson, “FFTW: An Adaptive Software Architecture for the FFT,” *Proceedings of the IEEE Conference on Acoustics, Speech, and Signal Processing (ICASS)*, 1998, pp. 1381–1384.

Received July 31, 2003; accepted for publication September 5, 2003

Dennis M. Newns *IBM Research Division, Thomas J. Watson Research Center, P.O. Box 218, Yorktown Heights, New York 10598 (dennism@us.ibm.com)*. Dr. Newns received his Ph.D. degree in physical chemistry from Imperial College, London, in 1967. He subsequently held research positions at the University of Chicago and Cambridge University, and then held academic positions at Imperial College until joining the research staff of IBM in 1986. Dr. Newns’ research interests, primarily in condensed matter, include surface science, the Kondo effect and heavy Fermion systems, high-temperature superconductivity, molecular biology, and most recently micromagnetics and quantum computation.

Wilm E. Donath Dr. Donath received his B.S. degree in chemical engineering from Carnegie Tech (now Carnegie Mellon University) and his Ph.D. degree from the University of California at Berkeley. He worked for IBM from 1958 to 2002, mainly in design automation. Dr. Donath is retired from IBM and is currently working on fluid dynamics.

Glenn J. Martyna *IBM Research Division, Thomas J. Watson Research Center, P.O. Box 218, Yorktown Heights, New York 10598 (gmartyna@ibm.com)*. Dr. Martyna received his Ph.D. degree in physics from Columbia University and became a National Science Foundation Postdoctoral Fellow in computational science and engineering at the University of Pennsylvania. He was a tenured faculty member at Indiana University, Bloomington, before joining IBM. Dr. Martyna’s research has focused on atomistic modeling of chemical, biological, and materials processes, and in particular, developing novel techniques that markedly increase the speed and efficiency of computer simulations and applying the methods to investigate important phenomena.

Manfred E. Schabes *Hitachi San Jose Research Center, 650 Harry Road, San Jose, California 95120 (manfred@almaden.ibm.com)*. Dr. Schabes is a Research Staff Member at the Research Division of Hitachi Global Storage Technologies. He received his Ph.D. degree in physics from the University of California at San Diego in 1989. After assignments at Honeywell and Komag, he joined the IBM Research Division in 1997 as a Research Staff Member at the Almaden Research Center, where he worked on micromagnetic theory of nonuniform magnetization processes in magnetic nanograins and thin films, and simulations of novel magnetic recording media architectures. Dr. Schabes received an IBM Outstanding Technical Achievement Award in 2002 for his contributions to the invention, development, and implementation of antiferromagnetically coupled magnetic recording media. He has several patents and many publications in the field of micromagnetic theory and magnetic recording technology. Dr. Schabes is a member of the American Physical Society and the Institute of Electrical and Electronics Engineers.

Byron H. Lengsfeld III *Hitachi San Jose Research Center, 650 Harry Road, San Jose, California 95120 (byron.lengsfeldiii@hgst.com)*. Dr. Lengsfeld received a B.S. degree from the University of the South in 1974 and a Ph.D. degree in physical chemistry from the Virginia Polytechnic Institute and State University in 1978. From 1978 to 1980 he was a National Research Council Postdoctoral Fellow at the

NASA Langley Research Center, where he developed second-order MCSCF algorithms. From 1980 until 1982 he worked at the IBM San Jose Research Center and is one of the co-authors of the Alchemy II electronic structure package. From 1982 to 1987 he held a research position at the U.S. Army Aberdeen Proving Grounds, where he developed computational techniques to analytically determine derivatives of MCSCF and multi-reference CI wavefunctions. From 1988 to 1992 he was a staff scientist in the Theoretical Atomic and Molecular Physics Group at Lawrence Livermore National Laboratory, where he worked on the development of an electron-molecule scattering/molecular photoionization code based on the complex-Kohn method. In 1992 Dr. Lengsfeld became a Research Staff Member at the IBM Almaden Research Center, where his work centered on electronic structure theory. In 2000 he joined the Magnetic Theory and Modeling Group at the IBM Almaden Research Center.